



Jones pupil decomposition and its lithographic imaging impacts

ZHIYUAN NIU,^{1,5}  MING DING,¹ JUNHAI JIANG,² HONGBO SHANG,^{3,4} SIYU ZHU,^{1,4} FANG ZHANG,¹ WEIJIE SHI,² AIJUN ZENG,^{1,4} AND HUIJIE HUANG^{1,4,6}

¹Laboratory of Information Optics and Optoelectronic Technology, Shanghai Institute of Optics and Fine Mechanics, Chinese Academy of Sciences, Shanghai 201800, China

²Dongfang Jingyuan Electron Ltd., Beijing 100176, China

³Changchun Institute of Optics, Fine Mechanics and Physics, Chinese Academy of Sciences, Changchun 130033, China

⁴University of Chinese Academy of Sciences, Beijing 100049, China

⁵e-mail: niuzhiyuan_pku@163.com

⁶e-mail: huanghuijie@siom.ac.cn

Received 5 November 2020; revised 12 January 2021; accepted 13 January 2021; posted 13 January 2021 (Doc. ID 414144); published 9 February 2021

The Jones pupil is a full description of imaging properties of projection lenses in optical lithography. The decomposition of the Jones pupil into components with clear physical meanings was studied previously; however, the decomposition method has not been studied systematically. To generalize the existing decomposition method, this work is aimed at finding all the decomposition methods and analyzing the lithographic imaging impacts. In this work, six decomposition methods are proposed, and the lithographic imaging impacts of the Jones components are studied and compared for all the decomposition methods. The results demonstrate that, although the decomposition methods are different, their lithographic impacts are identical. To be specific, apodization has a dominant impact on the critical dimension with a magnitude of 1.3 nm, and the impact of diattenuation is 0.3 nm. In contrast, the impacts of the other Jones components of aberration, birefringence, rotator, and ellipticity are negligible. This work gives a complete understanding of the imaging impacts of the Jones pupil. © 2021 Optical Society of America

<https://doi.org/10.1364/AO.414144>

1. INTRODUCTION

With the evolution of immersion lithography, the numerical aperture (NA) of the projection lens keeps growing and reaches up to 1.35 nowadays. For the hyper-NA ($NA > 1$) lithographic process, vectorial imaging needs to be considered for accurate modeling by including the polarization effects [1,2]. For scalar imaging, the imaging properties of the projection lens are characterized by a transmission map and a phase map, while for vectorial imaging, these two maps should be replaced by the Jones pupil, which assigns a 2×2 complex Jones matrix at each pupil location. Due to a lack of direct physical meanings, the Jones pupil decomposition into components that represent a clear physical interpretation and are realizable by optical elements has been discussed and well understood in previous literatures. Lu and Chipman extracted the diattenuation and retardation properties from inhomogeneous polarization elements by the method of singular-value decomposition (SVD) [3]. McIntyre, Levinson, and Neureuther gave a comparison of the Mueller pupil, the Jones pupil, and the Pauli pupil, where the Jones pupil is decomposed as a sum of Pauli spin matrices [4]. But the Pauli decomposition still lacks physical meanings, as the total Jones matrix of sequencing of various optical

elements is mathematically described by multiplication, not summation as in Pauli decomposition. Barakat provided several basic theorems of decomposition of the Jones matrix [5], which stated that a Jones matrix could be expressed as the product of two rotators, two retarders, and one partial polarizer. Geh *et al.* gave the most appropriate decomposition method for the lithographic lens and studied the imaging impact of the decomposed components [6], which showed that the Jones matrix could be expressed as the product of three elementary Jones matrices, a rotated partial polarizer, a rotator, and a retarder, together with a scalar transmission and a phase factor, and that apodization and diattenuation were the main contributors to lithographic imaging variation in all the Jones components. As a generalization of the scalar Zernike polynomials, Ruoff and Totzeck introduced orientation Zernike polynomials to describe diattenuation and retardation [7,8], based on which Zhou *et al.* studied the birefringence caused by calcium fluoride [9], and Shang *et al.* established the method of lens clocking optimization [10]. Now two natural questions come up: are there any other decomposition methods of the Jones pupil, and are the imaging impacts of Jones components the same for these different decomposition methods? Based on Ref. [6], our goal is to generalize the existing decomposition method and to find all

possible decomposition methods that consist of basic physical quantities such as apodization, diattenuation, scalar aberrations, rotator, and retardation, and to study the lithographic imaging impacts for these decomposition methods. Apodization accounts for the average transmittivity of the two orthogonal field components, which is usually caused by bulk absorption of the lens material and coatings. Diattenuation means the transmittivity split for the two orthogonal field components, which can be realized by a partial polarizer. Scalar aberrations are caused by residual aberrations in lens design, refractive index fluctuations of lens material, and surface figure deviations of the lens elements. It is usually expanded in Zernike polynomials in imaging calculation. The rotator rotates the linear polarization state in counterclockwise direction for a certain angle, and retardation (or birefringence) is realized by a retarder, which assigns different phase changes to the orthogonal field components.

This work is organized as follows: Section 2 introduces the mathematical description of Jones pupil decomposition. Based on SVD, different decomposition methods are discussed and compared. In Section 3, the decomposition methods are applied to a typical Jones pupil of a lithographic projection lens. The imaging impacts of decomposed components are simulated and compared for all decomposition methods. We conclude the results in Section 4 with a summary.

2. JONES PUPIL DECOMPOSITION

The Jones matrix is a 2×2 complex matrix with eight independent parameters and defined by

$$\begin{pmatrix} E_{\text{out},x} \\ E_{\text{out},y} \end{pmatrix} = \begin{pmatrix} J_{xx} & J_{xy} \\ J_{yx} & J_{yy} \end{pmatrix} \begin{pmatrix} E_{\text{in},x} \\ E_{\text{in},y} \end{pmatrix}. \quad (1)$$

It contains full information about the polarization properties of the optical element. The three basic optical elements are the partial polarizer, which attenuates or completely blocks one polarization component; the retarder, which induces a phase shift between two orthogonal field components; and the rotator, which rotates a linear polarization state counterclockwise by a certain angle.

For the partial polarizer, retarder, and rotator, the Jones matrices are given by

$$J_{\text{pol}}(t, d) = t J_{\text{pol}}(d) = t \begin{pmatrix} 1+d & 0 \\ 0 & 1-d \end{pmatrix}, \quad (2)$$

$$J_{\text{ret}}(\Phi, \phi) = e^{i\Phi} J_{\text{ret}}(\phi) = e^{i\Phi} \begin{pmatrix} e^{-i\phi} & 0 \\ 0 & e^{i\phi} \end{pmatrix}, \quad (3)$$

$$J_{\text{rot}}(\theta) = \begin{pmatrix} \cos\theta & -\sin\theta \\ \sin\theta & \cos\theta \end{pmatrix}. \quad (4)$$

With these definitions, for the partial polarizer, t and $2d$ are the mean amplitude transmission and the relative transmission difference of the amplitude, and they represent apodization and diattenuation, respectively. They are related to the more commonly used intensity-based transmission T and diattenuation D through

$$T = t^2(1 + d^2), \quad (5)$$

$$D = \frac{2d}{1 + d^2}. \quad (6)$$

The retarder is characterized by a global phase Φ and a retardation 2ϕ with the fast axis, which represent the scalar aberration and birefringence. The scalar aberration represents the mean phase of the two orthogonal field components, and the birefringence means the phase difference of the two orthogonal field components. The rotator rotates the linear polarization state in counterclockwise direction for a positive angle θ . Since the mean transmission t in Eq. (2) and phase Φ in Eq. (3) are separable scalar quantities, we will omit them in the Jones matrices in the following discussion. The Jones matrices of a rotated partial polarizer and rotated retarder are obtained by taking the similarity transform, and given by

$$\begin{aligned} J_{\text{pol}}(d, \theta) &= J_{\text{rot}}(\theta) \begin{pmatrix} 1+d & 0 \\ 0 & 1-d \end{pmatrix} J_{\text{rot}}(-\theta) \\ &= \begin{pmatrix} 1+d\cos 2\theta & d\sin 2\theta \\ d\sin 2\theta & 1-d\cos 2\theta \end{pmatrix}, \end{aligned} \quad (7)$$

$$\begin{aligned} J_{\text{ret}}(\phi, \theta) &= J_{\text{rot}}(\theta) \begin{pmatrix} e^{-i\phi} & 0 \\ 0 & e^{i\phi} \end{pmatrix} J_{\text{rot}}(-\theta) \\ &= \begin{pmatrix} \cos\phi - i\sin\phi\cos 2\theta & -i\sin\phi\sin 2\theta \\ -i\sin\phi\sin 2\theta & \cos\phi + i\sin\phi\cos 2\theta \end{pmatrix}. \end{aligned} \quad (8)$$

By taking the SVD, the Jones matrix can be decomposed as

$$\begin{aligned} J &= USV^\dagger = (USU^\dagger)(UV^\dagger) = J_{\text{H1}}J_{\text{U}}, \\ &= (UV^\dagger)(VSV^\dagger) = J_{\text{U}}J_{\text{H2}}, \end{aligned} \quad (9)$$

where U and V are unitary matrices, S is the diagonal matrix containing the positive real singular values, $J_{\text{H1}} = USU^\dagger$ and $J_{\text{H2}} = VSV^\dagger$ are positive definite Hermitian matrices, and $J_{\text{U}} = UV^\dagger$ is a unitary matrix. Equation (9) is polar decomposition, by which an eight-parameter Jones matrix is expressed as the product of a four-parameter Hermitian matrix and a four-parameter unitary matrix. Note that the unitary matrix J_{U} is the same in Eq. (9), whether being at first or second place in the decomposition.

Let us first consider the four-parameter decomposition of the Hermitian matrix J_{H1} , which is derived in Appendix A and given by

$$\begin{aligned} J_{\text{H1}}(t, d, \theta_1, \delta_1) &= t J_{\text{ret}}\left(\frac{\delta_1}{2}\right) J_{\text{pol}}(d, \theta_1) J_{\text{ret}}\left(-\frac{\delta_1}{2}\right) \\ &= t \begin{pmatrix} 1+d\cos 2\theta_1 & e^{-i\delta_1}d\sin 2\theta_1 \\ e^{i\delta_1}d\sin 2\theta_1 & 1-d\cos 2\theta_1 \end{pmatrix}, \end{aligned} \quad (10)$$

where θ_1 is the rotation angle of partial polarizer, and δ_1 is the ellipticity parameter. Similarly, the decomposition of J_{H2} is given by

$$\begin{aligned} J_{\text{H2}}(t, d, \theta_2, \delta_2) &= t J_{\text{ret}}\left(\frac{\delta_2}{2}\right) J_{\text{pol}}(d, \theta_2) J_{\text{ret}}\left(-\frac{\delta_2}{2}\right) \\ &= t \begin{pmatrix} 1+d\cos 2\theta_2 & e^{-i\delta_2}d\sin 2\theta_2 \\ e^{-i\delta_2}d\sin 2\theta_2 & 1-d\cos 2\theta_2 \end{pmatrix}. \end{aligned} \quad (11)$$

J_{H1} and J_{H2} share the same t and d , but different θ and δ . The difference of J_{H1} and J_{H2} is given by

$$J_{\text{H1}}^2 - J_{\text{H2}}^2 = JJ^\dagger - J^\dagger J. \quad (12)$$

Only when the Jones matrix is a normal matrix, i.e., $JJ^\dagger = J^\dagger J$, does $J_{H1} = J_{H2}$. Since J is very close to the identity matrix I , it can be written as

$$J = I + \Delta, \tag{13}$$

where Δ is a complex matrix with small elements. Equation (12) can be processed into

$$J_{H1}^2 - J_{H2}^2 = \Delta\Delta^\dagger - \Delta^\dagger\Delta = O(\Delta^2), \tag{14}$$

which means that with smaller Δ , J_{H1} is closer to J_{H2} .

Now consider the four-parameter decomposition of the unitary matrix J_U . Three decomposition methods for a unitary matrix are derived in Appendix A, and given by

$$\begin{aligned} J_{U1}(\Phi, \tau, \phi, \gamma) &= e^{i\Phi} J_{\text{ret}}\left(\frac{\tau}{2}\right) J_{\text{ret}}(\phi, \gamma) J_{\text{ret}}\left(-\frac{\tau}{2}\right) \\ &= e^{-i\Phi} \begin{pmatrix} \cos \phi - i \sin \phi \cos 2\gamma & -ie^{-i\tau} \sin \phi \sin 2\gamma \\ -ie^{i\tau} \sin \phi \sin 2\gamma & \cos \phi + i \sin \phi \cos 2\gamma \end{pmatrix}, \end{aligned} \tag{15}$$

$$\begin{aligned} J_{U2}(\Phi, \alpha, \varphi, \beta) &= e^{i\Phi} J_{\text{rot}}(\alpha) J_{\text{ret}}(\varphi, \beta) \\ &= e^{i\Phi} \begin{pmatrix} \cos \varphi \cos \alpha - i \sin \varphi \cos(\alpha + 2\beta) & -\cos \varphi \sin \alpha - i \sin \varphi \sin(\alpha + 2\beta) \\ \cos \varphi \sin \alpha - i \sin \varphi \sin(\alpha + 2\beta) & \cos \varphi \cos \alpha + i \sin \varphi \cos(\alpha + 2\beta) \end{pmatrix}, \end{aligned} \tag{16}$$

and

$$\begin{aligned} J_{U3}(\Phi, \rho, \vartheta, \sigma) &= e^{i\Phi} J_{\text{ret}}(\rho) J_{\text{rot}}(\vartheta) J_{\text{ret}}(\sigma) \\ &= e^{i\Phi} \begin{pmatrix} e^{-i(\rho+\sigma)} \cos \vartheta & -e^{-i(\rho-\sigma)} \sin \vartheta \\ e^{i(\rho-\sigma)} \sin \vartheta & e^{i(\rho+\sigma)} \cos \vartheta \end{pmatrix}. \end{aligned} \tag{17}$$

As mentioned in Eq. (9), the unitary matrix J_U is uniquely determined in polar decomposition. It is worth noting that we just use the three notations J_{U1} , J_{U2} , and J_{U3} in Eqs. (15)–(17) to represent the three different decomposition methods for the same J_U . Besides the global phase term, Eq. (15) consists of three retarders. Equation (16) consists of a rotator and a retarder, which was first derived by Poincaré [11] and called Poincaré decomposition [6], and Eq. (17) is a retarder–rotator–retarder (called Euler parameterization) mode known in group theory [12]. Then the six decomposition methods are given by

$$J = J_{H1}J_{U1} = J_{H1}J_{U2} = J_{H1}J_{U3} = J_{U1}J_{H2} = J_{U2}J_{H2} = J_{U3}J_{H2}. \tag{18}$$

It should be noted that apodization t , diattenuation d , and global phase Φ are independent of decomposition methods in Eq. (18).

In Ref. [6], the decomposition method $J = J_{H1}J_{U2}$ is discussed and used to perform the lithographic simulation. As a generalization of Ref. [6], in this paper, the differences between J_{H1} and J_{H2} are compared and discussed, and more importantly, three different decomposition methods for J_U are proposed and discussed. The lithographic simulations are performed for all six decomposition methods to draw a more general conclusion.

3. DECOMPOSITION RESULTS AND IMPACT ON LITHOGRAPHY IMAGING

A. Decomposition and Reconstruction of Jones Pupil

The decomposition methods are applied to a typical Jones pupil of a lithographic projection lens, which is illustrated in Fig. 1.

The Jones pupil in Fig. 1 is from a real design of a lithographic projection lens based on Ref. [13]. CODE V optical design software is used to extract the Jones pupil. The Jones pupil, which assigns a 2×2 complex Jones matrix at each pupil location, can be written as

$$J(p_x, p_y) = \begin{pmatrix} J_{xx}(p_x, p_y) & J_{xy}(p_x, p_y) \\ J_{yx}(p_x, p_y) & J_{yy}(p_x, p_y) \end{pmatrix}, \tag{19}$$

where p_x and p_y are the normalized pupil locations with respect to NA. For each complex matrix element, the real part and imaginary part are plotted as a function of normalized pupil coordinates (p_x, p_y) , so we get eight maps in Fig. 1. In the following, all the decomposed parameters are plotted as a function of (p_x, p_y) implicitly.

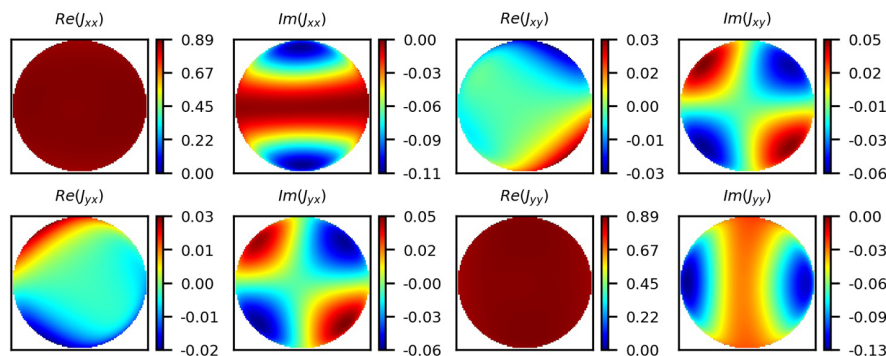


Fig. 1. Typical Jones pupil of a lithographic projection lens with eight independent maps. The ideal maps are the identity matrix with only $\text{Re}(J_{xx}) = 1$ and $\text{Re}(J_{yy}) = 1$. Due to non-perfection, the real maps have small deviations.

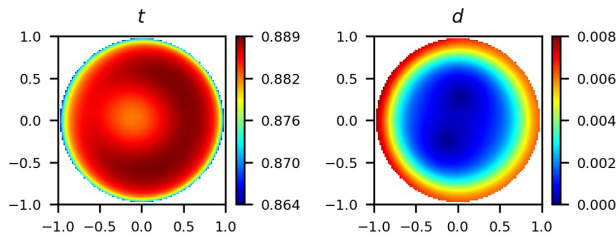


Fig. 2. Left: apodization map. Right: diattenuation map.

First the Hermitian matrix decomposition is discussed. The apodization map and diattenuation map are the same between J_{H1} and J_{H2} , and shown in Fig. 2.

The apodization map has an average value of 0.884, which seems a big deviation from the ideal value of one (since the ideal Jones matrix is just the identity matrix). Since this average value of apodization blocks the energy uniformly, we can always get the same lithographic imaging by increasing the energy. Compared with the average transmission, the apodization uniformity affects the lithographic imaging more. As shown in Fig. 2, the apodization uniformity has a peak-to-valley (PV) value of 0.025, and the diattenuation map has an average value of 0.004. Later we will see that apodization and diattenuation are the two main contributors to the lithographic imaging.

The other two parameters (δ , θ) are shown and compared in Fig. 3.

As can be seen in Fig. 3, the rotation angle θ of the partial polarizer has approximately central symmetry in the pupil. The θ maps of J_{H1} and J_{H2} are almost the same, and the difference map of $\theta_1 - \theta_2$ are small, with a magnitude of less than 1.5° . For the ellipticity parameters δ , the values are small for most pupil areas but large for some small areas, where θ is near 0° and 90°

in the θ map. In Eq. (10) or Eq. (11), the ellipticity parameter δ is extracted from the term $e^{i\delta} d \sin 2\theta$. The diattenuation parameter d is small and less than 0.008 in Fig. 2. When $\theta \rightarrow 0^\circ$ or $\theta \rightarrow 90^\circ$, $d \sin 2\theta \rightarrow 0$. Under these cases, the δ extraction is meaningless. In other words, although the value of δ is large in these areas, it has no impact on the accuracy of the decomposition. Later we will show that ellipticity has little impact on lithographic imaging.

Now consider the unitary matrix decomposition. According to Appendix A, the unitary matrix can be decomposed as the product of a phase term and a special unitary matrix, given by $J_U = e^{i\Phi} \tilde{U}$. The phase term is independent of the decomposition methods and shown in Fig. 4.

As expected, the scalar aberration is very small with a magnitude of several milli-wavelength. Here one milli-wavelength means 0.1% of wavelength, which is 0.193 nm for modern deep ultraviolet (DUV) scanners with $\lambda = 193$ nm.

The special unitary part \tilde{U} is very close to the identity matrix. The difference of them is shown in Fig. 5.

In Fig. 5, it can be seen that the difference between \tilde{U} and the identity matrix is of order 10^{-2} . The other three parameters, (τ, ϕ, γ) of J_{U1} , (α, φ, β) of J_{U2} , and $(\vartheta, \rho, \sigma)$ of J_{U3} , can be extracted in the three different decomposition methods, shown in Fig. 6.

As shown in Fig. 6, for $J_{U1}(\Phi, \tau, \phi, \gamma)$, the τ map is similar to the δ map of J_H , whose value is relatively large for the areas where $\gamma \rightarrow 0^\circ$ and $\gamma \rightarrow 90^\circ$ due to the term $e^{i\tau} \sin \phi \sin 2\gamma$ in Eq. (15). The retardation map of ϕ is small and less than 4° . The ϕ and γ maps have approximately central symmetry. For $J_{U2}(\Phi, \alpha, \varphi, \beta)$, the rotation angle α of the rotator is small and less than 1.4° . The φ and β maps of J_{U2} are similar to the ϕ and γ maps of J_{U1} , respectively. Recall the detailed decompositions of J_{U1} and J_{U2} , which are given by

$$\begin{aligned}
 J_{U1} &= e^{i\Phi} J_{\text{ret}} \left(\frac{\tau}{2} \right) J_{\text{ret}} (\phi, \gamma) J_{\text{ret}} \left(-\frac{\tau}{2} \right) \\
 &= e^{i\Phi} \begin{pmatrix} \cos \phi - i \sin \phi \cos 2\gamma & -\sin \phi \sin 2\gamma (\sin \tau + i \cos \tau) \\ \sin \phi \sin 2\gamma (\sin \tau - i \cos \tau) & \cos \phi + i \sin \phi \cos 2\gamma \end{pmatrix}
 \end{aligned} \tag{20}$$

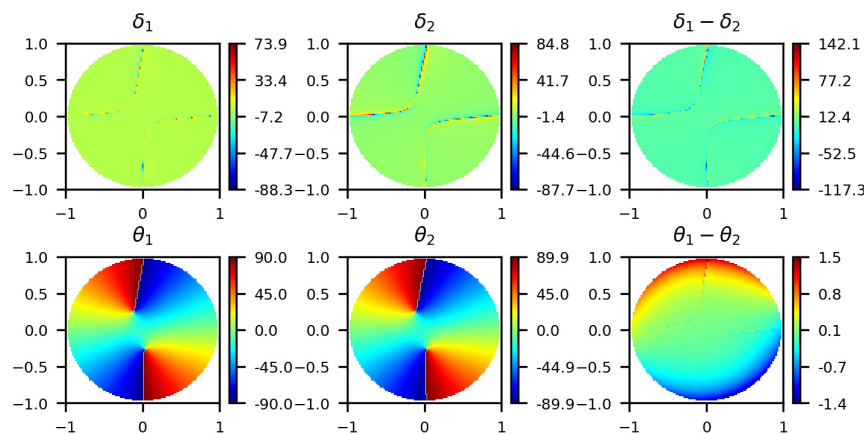


Fig. 3. Left column: δ_1 and θ_1 map of J_{H1} . Middle column: δ_2 and θ_2 map of J_{H2} . Right column: difference maps of δ_1 and δ_2 , θ_1 and θ_2 . All parameters are in unit of degree.

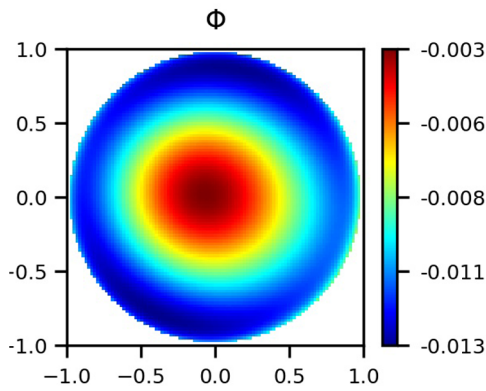


Fig. 4. Scalar phase aberrations in unit of wavelength; as can be seen, the aberration is several milli-wavelength.

and

$$\begin{aligned}
 J_{U2} &= e^{i\Phi} J_{\text{rot}}(\alpha) J_{\text{ret}}(\varphi, \beta) \\
 &= e^{i\Phi} \begin{pmatrix} \cos \varphi \cos \alpha - i \sin \varphi \cos(\alpha + 2\beta) & -\cos \varphi \sin \alpha - i \sin \varphi \sin(\alpha + 2\beta) \\ \cos \varphi \sin \alpha - i \sin \varphi \sin(\alpha + 2\beta) & \cos \varphi \cos \alpha + i \sin \varphi \cos(\alpha + 2\beta) \end{pmatrix}. \tag{21}
 \end{aligned}$$

As previously mentioned, J_{U1} and J_{U2} are just two different decompositions for the same J_U , so $J_{U1} = J_{U2} = J_U$. For small α , ϕ , and φ , the relations $\varphi \simeq \phi$ and $\beta \simeq \gamma$ are satisfied.

For $J_{U3}(\Phi, \rho, \vartheta, \sigma)$, the rotation angle of the rotator ϑ is small, with a magnitude of 3.8° , and the ϑ map is approximately central antisymmetric. The detailed decompositions of J_{U3} is given by

$$\begin{aligned}
 J_{U3} &= e^{i\Phi} J_{\text{ret}}(\rho) J_{\text{rot}}(\vartheta) J_{\text{ret}}(\sigma) \\
 &= e^{i\Phi} \begin{pmatrix} \cos \vartheta \cos(\rho + \sigma) - i \cos \vartheta \sin(\rho + \sigma) & -\sin \vartheta \cos(\rho - \sigma) + i \sin \vartheta \sin(\rho - \sigma) \\ \sin \vartheta \cos(\rho - \sigma) + i \sin \vartheta \sin(\rho - \sigma) & \cos \vartheta \cos(\rho + \sigma) + i \cos \vartheta \sin(\rho + \sigma) \end{pmatrix}. \tag{22}
 \end{aligned}$$

It can be seen that parameters ρ and σ are involved in Eq. (22) by the combination of $\rho + \sigma$ or $\rho - \sigma$. In Fig. 5, we see that $\text{Re}(J_{xx}) = \cos \vartheta \cos(\rho + \sigma)$ is very close to one, which requires that $\vartheta \approx 0$ and $\rho + \sigma \approx 0$. That is why the ρ map and σ map have opposite values. In Fig. 6, ρ is near $+45^\circ$ or -45° , and σ is near -45° or $+45^\circ$ accordingly.

In addition, the six decomposition methods are validated by comparing the reconstructed Jones pupil and the original Jones pupil. In Fig. 1, it can be seen the Jones pupil is close to

the identity matrix with a magnitude of one. The differences between the reconstructed Jones pupil and the original Jones pupil are about 10^{-7} , which is a negligible value with respect to a magnitude of one, and this proves that the decomposition methods are valid.

B. Lithographic Imaging Impacts of Jones Pupil Components

The schematic diagram of the lithographic process is shown in Fig. 7.

The light from the illumination, with predefined wavelength, intensity, direction, and polarization, illuminates at the mask located at the object plane, and then is diffracted. The diffracted light is collected by the projection lens, whose imaging property includes the NA and the Jones pupil. The mask makes its

image at the wafer located on the image plane. In real cases, the light illuminates at the mask from many different directions. The lights from different directions are incoherent. To get the final mask image on the wafer, the image for each direction is calculated coherently, and then the images for all the directions are summed up incoherently. The critical dimension (CD) is calculated based on the final image, shown in Fig. 8.

Table 1 provides the simulation conditions.

The optical proximity effect (OPE) curve is the CD plot of the through pitch patterns (usually the tightest CD; here it is $L = 45 \text{ nm}$), which is an important curve in lithography to see the OPE. By judging the CD differences of the OPE curve, we can see how largely a factor affects the lithographic process. For the 28 nm technology node and below, if the CD differences of

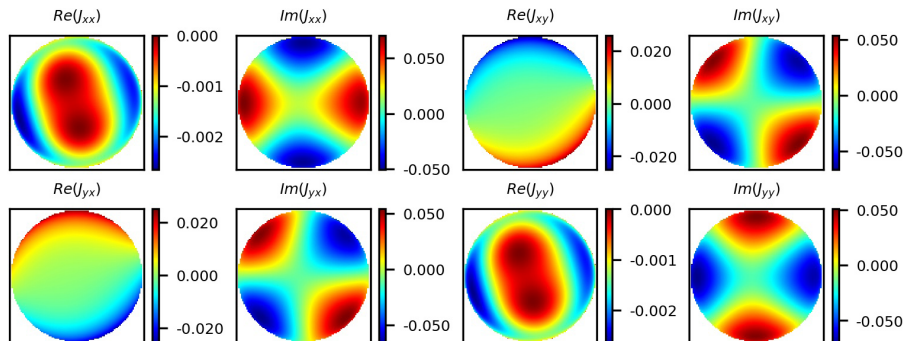


Fig. 5. Difference map of special unitary matrix \tilde{U} and the identity matrix.

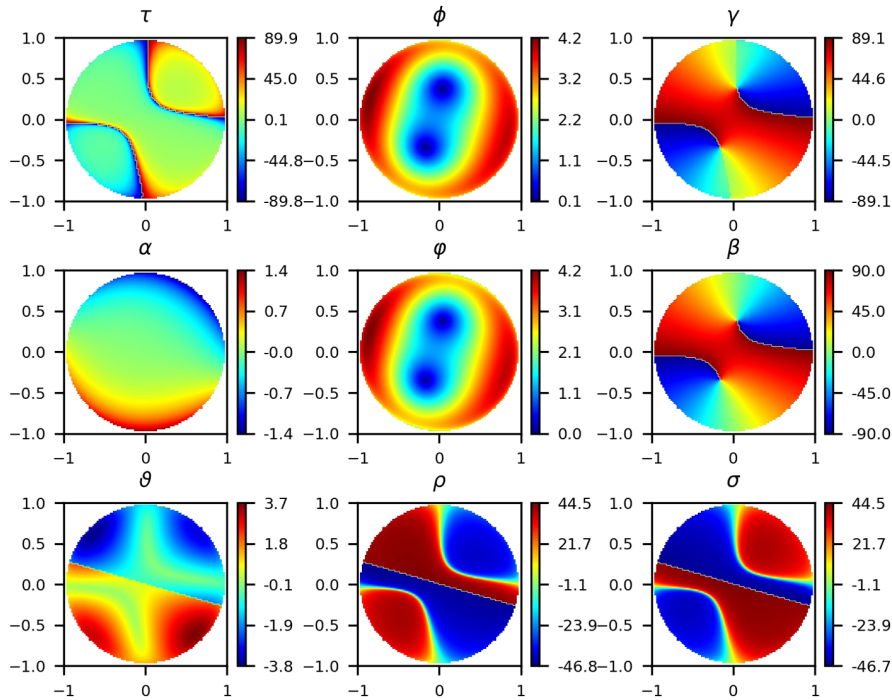


Fig. 6. Different decomposition methods of the unitary matrix: $J_{U1}(\tau, \phi, \gamma)$, $J_{U2}(\alpha, \phi, \beta)$, and $J_{U3}(\theta, \rho, \sigma)$. All parameters are in unit of degree.

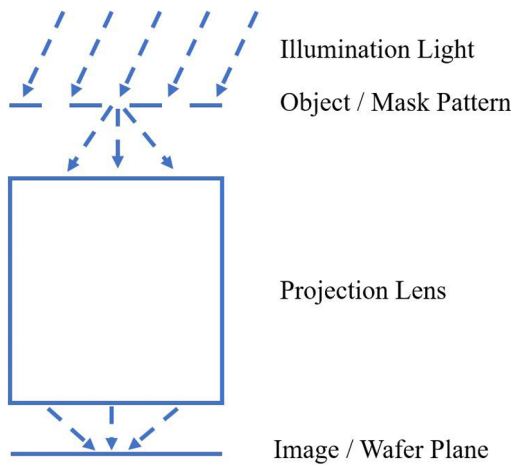


Fig. 7. Schematic diagram of lithographic imaging.

the OPE curve caused by one factor are a magnitude of 1 nm, this factor should be considered for accurate lithographic modeling. To study the impact of apodization, the Jones pupil is reconstructed without the apodization parameter only. The OPE curves are simulated with the reconstructed Jones pupil and the full Jones pupil, and the CD differences of the OPE curves are obtained by comparing the two. The bigger the CD differences are, the more impacts the apodization contributes. The CD differences of the OPE curve for apodization, aberration, and diattenuation are shown in Fig. 11.

Similarly, the impacts of other parameters are analyzed with the same method. We define the maximum CD difference as the PV value of the CD differences of the OPE curve, e.g., the CD differences of the apodization in Fig. 11 range from -0.1

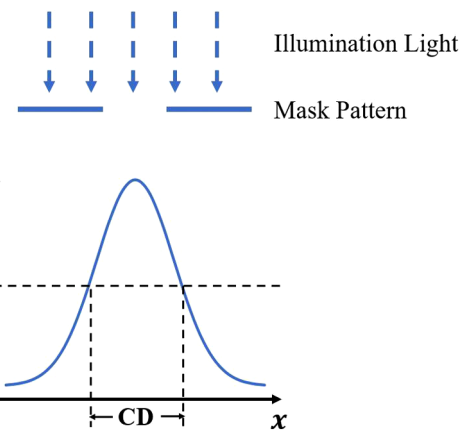


Fig. 8. CD is defined as the distance between the two points satisfying the equation $I(x) = I_0$, where I_0 is the threshold determined by a predefined mask pattern L45P90, whose CD is exactly 45 nm at I_0 . Then the CDs of other patterns can be calculated at I_0 .

to 1.2 nm, then the maximum CD difference of apodization is 1.3 nm. The maximum CD differences contributed by the Jones components are summarized in Table 2.

As discussed in Section 2, apodization t , diattenuation d , and scalar aberration Φ are independent of decomposition methods.

In Table 2, although the decomposition methods are different, the CD impacts of ellipticity, birefringence, and rotator are almost the same, which are about 0.0 nm, 0.1 nm, and 0.0 nm, respectively. The maximum CD differences of the Jones components are summarized in Fig. 12.

From the studied case, apodization has a dominant impact on CD with a value of 1.3 nm. The impact of diattenuation on CD is 0.3 nm. In contrast, the impacts of the scalar aberration,

Table 1. Lithography Simulation Conditions

Name	Value/Description
Wavelength (nm)	193. Wavelength of illuminated light.
Numerical aperture	1.35. NA of the projection lens.
Illumination type	Freeform illumination with intensity map shown in Fig. 9. The intensity map is plotted as function of the pupil coordinates.
Polarization	XY. The polarization type is XY, which is a widely used polarization mode in modern lithography.
Mask	6% attenuated phase shifting mask (attPSM), dark field. The mask has 100% transmission and no phase change for the pattern areas, and has 6% transmission and phase change of 180° for the other areas (called background or field areas).
Patterns	Through pitch patterns with line $L = 45$ nm, pitch $P = 90 - 400$ nm. The patterns are corrected with OPC (optical proximity correction) to print size to target. The pattern is shown in Fig. 10. Due to diffraction, the shape of mask image is usually far different from that of mask. OPC is a technique to optimize the mask pattern's shape to get good image quality and the desired pattern shape.
Resist model	Pure optical model with threshold at which the pattern L45P90 is printed to 45 nm at wafer. The resist information is not taken into account. CDs calculated by this kind of model are called optical CDs.
Jones pupil	Original Jones pupil and 17 reconstructed ones.

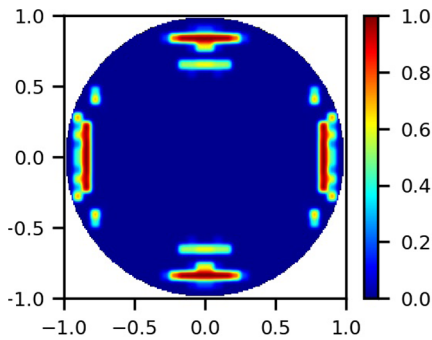


Fig. 9. Intensity map of freeform illumination as a function of the pupil coordinates.

birefringence, rotator, and ellipticity are negligible with less than 0.1 nm. These results are independent of decomposition methods and demonstrate that the imaging properties of the lithographic projection lens are almost fully characterized by apodization and diattenuation. The results also reveal that the imaging impacts of other Jones components are negligible.

4. SUMMARY

In this work, we generalized the Jones pupil decomposition method in Ref. [6] and got six different decomposition methods. With polar decomposition, the Jones matrix with eight parameters is expressed as the product of the Hermitian matrix and the unitary matrix, each with four parameters. The Hermitian matrix has two different forms, depending on

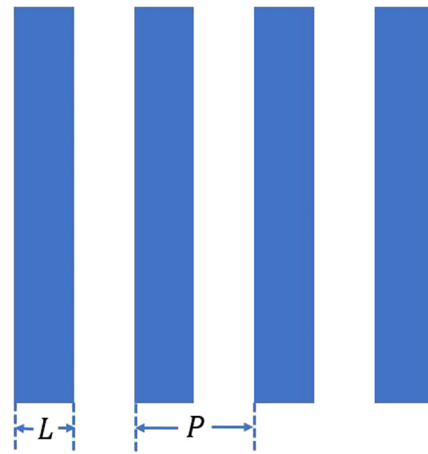


Fig. 10. Mask pattern of line pitch type. The line width is L , and the pitch is P . Many patterns of this type are simulated. For the same $L = 45$ nm, P ranges from 90 to 400 nm. The group of these patterns is called through pitch patterns.

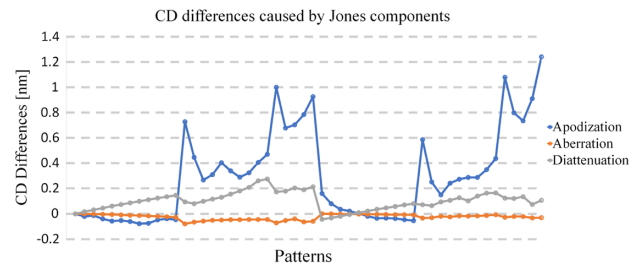


Fig. 11. CD differences of the OPE curve caused by apodization, aberration, and diattenuation.

Table 2. Imaging Impacts of Jones Components

Components	Max. CD Difference [nm]
(Apodization)	1.32
d (diattenuation)	0.32
Φ (aberration)	0.08
δ_1 of J_{H1} (ellipticity)	0.00
δ_2 of J_{H2} (ellipticity)	0.00
τ in $J = J_{H1}J_{U1}$ (ellipticity)	0.01
τ in $J = J_{U1}J_{H2}$ (ellipticity)	0.01
$J_{ret}(\phi, \gamma)$ in $J = J_{H1}J_{U1}$ (birefringence)	0.07
$J_{ret}(\phi, \gamma)$ in $J = J_{U1}J_{H2}$ (birefringence)	0.07
$J_{ret}(\varphi, \beta)$ in $J = J_{H1}J_{U2}$ (birefringence)	0.08
$J_{ret}(\varphi, \beta)$ in $J = J_{U2}J_{H2}$ (birefringence)	0.08
$J_{rot}(\alpha)$ in $J = J_{H1}J_{U2}$ (rotator)	0.01
$J_{rot}(\alpha)$ in $J = J_{U2}J_{H2}$ (rotator)	0.01
$J_{rot}(\vartheta)$ in $J = J_{H1}J_{U3}$ (rotator)	0.04
$J_{rot}(\vartheta)$ in $J = J_{U3}J_{H2}$ (rotator)	0.04
$J_{ret}(\rho)$ and $J_{ret}(\sigma)$ in $J = J_{H1}J_{U3}$ (birefringence)	0.07
$J_{ret}(\rho)$ and $J_{ret}(\sigma)$ in $J = J_{U3}J_{H2}$ (birefringence)	0.07

the position of the matrix product in the polar decomposition. The unitary matrix is uniquely determined in the polar decomposition, and has three decomposition methods. The first one consists of three retarders, the second one is a rotator-retarder

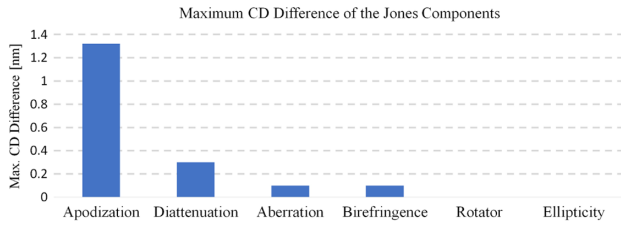


Fig. 12. Maximum CD differences contributed by the Jones components.

mode called Poincaré decomposition, and the third one is a retarder–rotator–retarder mode called Euler parameterization. The decomposition methods are validated by comparing the reconstructed Jones pupil and the original Jones pupil, and their differences are 10^{-7} , a negligible magnitude with respect to one. Furthermore, the lithographic imaging impacts are studied and compared for all the decomposition methods. The simulation results demonstrate that, for different decomposition methods, the imaging impacts of Jones components are identical. In the studied case, apodization and diattenuation are the main contributors to CD differences with magnitudes of 1.3 nm and 0.3 nm, respectively. However, the scalar aberration and birefringence bring negligible 0.1 nm CD differences, and the ellipticity and rotation contribute almost zero CD differences. The imaging properties of the lithographic projection lens are dominated by apodization and diattenuation. This work provides a deep and complete understanding of the Jones pupil impacts on lithographic imaging.

APPENDIX A: PARAMETERIZATION OF HERMITIAN MATRIX AND UNITARY MATRIX

A 2×2 complex matrix has four complex numbers, i.e., eight independent real parameters. For unitary matrices with the requirement

$$UU^\dagger = U^\dagger U = I, \quad (\text{A1})$$

the number of independent real conditions is four; thus, only $8-4=4$ independent parameters survive. The determinant of unitary matrices is derived from Eq. (A1) as

$$\det(U) = e^{i2\Phi}. \quad (\text{A2})$$

Here 2Φ is used for convenience of matrix decomposition in which the global phase term is $e^{i\Phi}$.

Unitary matrices with the requirement

$$\det(U) = 1 \quad (\text{A3})$$

are called special unitary matrices and have three independent parameters. Any 2×2 unitary matrix can be decomposed as the product of a phase term and a special unitary matrix, and is given by

$$U = e^{i\Phi} \tilde{U}, \quad (\text{A4})$$

where the special unitary matrix \tilde{U} can be parameterized with three parameters [6], and is given by

$$\tilde{U} = \begin{pmatrix} \cos \theta e^{i\mu} & -\sin \theta e^{i\nu} \\ \sin \theta e^{-i\nu} & \cos \theta e^{-i\mu} \end{pmatrix}. \quad (\text{A5})$$

Equation (A5) can be rewritten as

$$\begin{aligned} \tilde{U} &= \begin{pmatrix} \cos \theta & -\sin \theta e^{-i\delta} \\ \sin \theta e^{i\delta} & \cos \theta \end{pmatrix} \begin{pmatrix} e^{i\mu} & 0 \\ 0 & e^{-i\mu} \end{pmatrix} \\ &= \begin{pmatrix} \cos \theta e^{-i\delta} & -\sin \theta \\ \sin \theta & \cos \theta e^{i\delta} \end{pmatrix} \begin{pmatrix} e^{-i\nu} & 0 \\ 0 & e^{i\nu} \end{pmatrix}, \end{aligned} \quad (\text{A6})$$

where the ellipticity parameter is given by $\delta = -(\mu + \nu)$. The advantage of Eq. (A6) can be seen in the unitary similarity transform with the form

$$M = UDU^\dagger, \quad (\text{A7})$$

where D is a diagonal matrix $\text{diag}(c_1, c_2)$ with c_1 and c_2 as complex numbers. By application of Eq. (A6), Eq. (A7) is processed into

$$\begin{aligned} M &= UDU^\dagger = \tilde{U}D\tilde{U}^{-\dagger} \\ &= \begin{pmatrix} \cos \theta & -\sin \theta e^{-i\delta} \\ \sin \theta e^{i\delta} & \cos \theta \end{pmatrix} \begin{pmatrix} c_1 & 0 \\ 0 & c_2 \end{pmatrix} \begin{pmatrix} \cos \theta & \sin \theta e^{-i\delta} \\ -\sin \theta e^{i\delta} & \cos \theta \end{pmatrix} \\ &= \begin{pmatrix} \cos \theta e^{-i\delta} & -\sin \theta \\ \sin \theta & \cos \theta e^{i\delta} \end{pmatrix} \begin{pmatrix} c_1 & 0 \\ 0 & c_2 \end{pmatrix} \begin{pmatrix} \cos \theta e^{i\delta} & \sin \theta \\ -\sin \theta & \cos \theta e^{-i\delta} \end{pmatrix}. \end{aligned} \quad (\text{A8})$$

It can be seen that for a unitary matrix with four independent parameters $U(\Phi, \theta, \mu, \nu)$, only two parameters ($\theta, \delta = -(\mu + \nu)$) survive in the combination UDU^\dagger . In the unitary similarity transform of Eq. (A8), U can be simplified with two parameters and is written as

$$U = \begin{pmatrix} \cos \theta & -\sin \theta e^{-i\delta} \\ \sin \theta e^{i\delta} & \cos \theta \end{pmatrix} \quad (\text{A9})$$

or

$$U = \begin{pmatrix} \cos \theta e^{-i\delta} & -\sin \theta \\ \sin \theta & \cos \theta e^{i\delta} \end{pmatrix}. \quad (\text{A10})$$

It is convenient to rewrite Eq. (A9) as

$$\begin{aligned} U &= \begin{pmatrix} e^{-i\frac{\delta}{2}} & 0 \\ 0 & e^{i\frac{\delta}{2}} \end{pmatrix} \begin{pmatrix} \cos \theta & -\sin \theta \\ \sin \theta & \cos \theta \end{pmatrix} \begin{pmatrix} e^{i\frac{\delta}{2}} & 0 \\ 0 & e^{-i\frac{\delta}{2}} \end{pmatrix} \\ &= J_{\text{ret}} \left(\frac{\delta}{2} \right) J_{\text{rot}}(\theta) J_{\text{ret}} \left(-\frac{\delta}{2} \right) \end{aligned} \quad (\text{A11})$$

and rewrite Eq. (A10) as

$$\begin{aligned} U &= \begin{pmatrix} e^{-i\frac{\delta}{2}} & 0 \\ 0 & e^{i\frac{\delta}{2}} \end{pmatrix} \begin{pmatrix} \cos \theta & -\sin \theta \\ \sin \theta & \cos \theta \end{pmatrix} \begin{pmatrix} e^{-i\frac{\delta}{2}} & 0 \\ 0 & e^{i\frac{\delta}{2}} \end{pmatrix} \\ &= J_{\text{ret}} \left(\frac{\delta}{2} \right) J_{\text{rot}}(\theta) J_{\text{ret}} \left(\frac{\delta}{2} \right). \end{aligned} \quad (\text{A12})$$

Now consider the parameterization of the Hermitian matrix. Any Hermitian matrix J_H can always be diagonalized with a unitary matrix U , which is given by

$$J_H = U \begin{pmatrix} r_1 & 0 \\ 0 & r_2 \end{pmatrix} U^\dagger, \quad (\text{A13})$$

where r_1 and r_2 are two real eigenvalues of J_H . Since Eq. (A13) is a similarity transform, U has only two independent parameters. By application of Eq. (A11) or Eq. (A12), Eq. (A13) can be rewritten as

$$J_H = J_{\text{ret}} \left(\frac{\delta}{2} \right) J_{\text{rot}}(\theta) \begin{pmatrix} r_1 & 0 \\ 0 & r_2 \end{pmatrix} J_{\text{rot}}(-\theta) J_{\text{ret}} \left(-\frac{\delta}{2} \right) \\ = t J_{\text{ret}} \left(\frac{\delta}{2} \right) J_{\text{pol}}(d, \theta) J_{\text{ret}} \left(-\frac{\delta}{2} \right). \tag{A14}$$

In the last step, the relations $r_1 = t(1 + d)$, $r_2 = t(1 - d)$ and the definition of the rotated partial polarizer of Eq. (7) are used.

Now consider the parameterization of the unitary matrix. The first decomposition method is that any unitary matrix J_U can always be diagonalized with a unitary matrix U , which is given by

$$J_U = U \begin{pmatrix} e^{i\phi_1} & 0 \\ 0 & e^{i\phi_2} \end{pmatrix} U^\dagger. \tag{A15}$$

Similarly, by application of Eq. (A11) or Eq. (A12), Eq. (A15) can be rewritten as

$$J_{U1}(\Phi, \phi, \delta, \theta) = U \begin{pmatrix} e^{i\phi_1} & 0 \\ 0 & e^{i\phi_2} \end{pmatrix} U^\dagger \\ = e^{i\Phi} J_{\text{ret}} \left(\frac{\delta}{2} \right) J_{\text{ret}}(\phi, \theta) J_{\text{ret}} \left(-\frac{\delta}{2} \right). \tag{A16}$$

In the last step, we use the relations $\Phi = (\phi_1 + \phi_2)/2$, $\phi = (\phi_2 - \phi_1)/2$ and the definition of the rotated retarder of Eq. (8). The first decomposition consists of three retarders besides the global phase term.

The second decomposition method is from a known theorem in group theory [14] that states that a 2×2 special unitary matrix can always be decomposed as

$$\tilde{U}(\varphi, \theta_1, \theta_2) = J_{\text{mt}}(\theta_1) J_{\text{ret}}(\varphi) J_{\text{rot}}(\theta_2). \tag{A17}$$

The special unitary matrix can be represented by a retarder sandwiched between two rotators. Without loss of generality, we rewrite θ_1 and θ_2 as

$$\theta_1 = \alpha + \beta, \theta_2 = -\beta, \tag{A18}$$

and Eq. (A17) is processed into

$$\tilde{U}(\varphi, \alpha, \beta) = J_{\text{rot}}(\alpha + \beta) J_{\text{ret}}(\varphi) J_{\text{rot}}(-\beta) \\ = J_{\text{rot}}(\alpha) J_{\text{rot}}(\beta) J_{\text{ret}}(\varphi) J_{\text{rot}}(-\beta) \\ = J_{\text{rot}}(\alpha) J_{\text{ret}}(\varphi, \beta). \tag{A19}$$

Taking into account the global phase term, the second decomposition method of the unitary matrix is given by

$$J_{U2}(\Phi, \varphi, \alpha, \beta) = e^{i\Phi} J_{\text{rot}}(\alpha) J_{\text{ret}}(\varphi, \beta), \tag{A20}$$

which was first derived by Poincaré [11], and Eq. (A20) is called Poincaré decomposition in Ref. [6].

The third decomposition method is from a group theory [12] that states that a 2×2 special unitary matrix can always be decomposed as

$$\tilde{U}(\theta_1, \theta_2, \theta_3) = e^{i\sigma_z\theta_1} e^{i\sigma_y\theta_2} e^{i\sigma_z\theta_3} \\ = \begin{pmatrix} e^{i\theta_1} & 0 \\ 0 & e^{-i\theta_1} \end{pmatrix} \begin{pmatrix} \cos \theta_2 & -\sin \theta_2 \\ \sin \theta_2 & \cos \theta_2 \end{pmatrix} \begin{pmatrix} e^{i\theta_3} & 0 \\ 0 & e^{-i\theta_3} \end{pmatrix} \\ = J_{\text{ret}}(-\theta_1) J_{\text{rot}}(\theta_2) J_{\text{ret}}(-\theta_3), \tag{A21}$$

where σ_y and σ_z are the Pauli matrices, given by

$$\sigma_y = \begin{pmatrix} 0 & -i \\ i & 0 \end{pmatrix}, \sigma_z = \begin{pmatrix} 1 & 0 \\ 0 & -1 \end{pmatrix}. \tag{A22}$$

Equation (A21) is called Euler parameterization, in which the special unitary matrix is represented by a rotator sandwiched between two retarders. Without loss of generality, we define $\rho = -\theta_1$, $\vartheta = \theta_2$, $\sigma = -\theta_3$, and taking into account the global phase term, the unitary matrix is decomposed as

$$J_{U3}(\Phi, \rho, \vartheta, \sigma) = e^{i\Phi} J_{\text{ret}}(\rho) J_{\text{rot}}(\vartheta) J_{\text{ret}}(\sigma). \tag{A23}$$

Funding. Shanghai Natural Science Foundation (19ZR1464300); Shanghai Sailing Program (18YF1426500); National Natural Science Foundation of China (61805264).

Disclosures. The authors declare no conflicts of interest.

REFERENCES

1. M. Totzeck, P. Gräupner, T. Heil, A. Göhnermeier, O. Dittmann, D. Krähmer, V. Kamenov, J. Ruoff, and D. Flagello, "How to describe polarization influence on imaging," *Proc. SPIE* **5754**, 23–37 (2005).
2. D. Flagello, S. Hansen, B. Geh, and M. Totzeck, "Challenges with hyper-NA (NA > 1) polarized light lithography for sub $\lambda/4$ resolution," *Proc. SPIE* **5754**, 53–68 (2005).
3. S. Y. Lu and R. A. Chipman, "Homogeneous and inhomogeneous Jones matrices," *J. Opt. Soc. Am. A* **11**, 766–773 (1994).
4. G. R. McIntyre, J. K. H. Levinson, and A. R. Neureuther, "Polarization aberrations in hyper-numerical-aperture projection printing: a comparison of various representations," *J. Micro/Nanolithog. MEMS MOEMS* **5**, 033001 (2006).
5. R. Barakat, "Jones matrix equivalence theorems for polarization theory," *Eur. J. Phys.* **19**, 209–216 (1998).
6. B. Geh, J. Ruoff, J. Zimmermann, P. Gräupner, M. Totzeck, M. Mengel, U. Hempelmann, and E. Schmitt-Weaver, "The impact of projection lens polarization properties on lithographic process at hyper-NA," *Proc. SPIE* **6520**, 65200F (2007).
7. J. Ruoff and M. Totzeck, "Orientation Zernike polynomials: a useful way to describe the polarization effects of optical imaging systems," *J. Micro/Nanolithog. MEMS MOEMS* **8**, 031404 (2009).
8. J. Ruoff and M. Totzeck, "Using orientation Zernike polynomials to predict the imaging performance of optical systems with birefringent and partly polarizing components," *Proc. SPIE* **7652**, 76521T (2010).
9. Z. Zhou, H. Shang, Y. Sui, and H. Yang, "Useful way to compensate for intrinsic birefringence caused by calcium fluoride in optical lithography systems," *Chin. Opt. Lett.* **16**, 032201 (2018).
10. H. Shang, L. Zhang, C. Liu, P. Wang, Y. Sui, and H. Yang, "Optimization based on sensitivity for material birefringence in projection lens," *Chin. Opt. Lett.* **18**, 062201 (2020).
11. H. Poincaré, *Theorie Mathematique de la Lumiere* (Cauthier-Villars, 1892), Vol. **2**, Chap. 12.
12. Y. M. Shnir, "Representations of SU(2)," in *Magnetic Monopoles* (Springer, 2005), pp. 501–504.
13. D. Shafer, A. Epple, A. Dodoc, W. Ulrich, and K. H. Schuster, "Catadioptric projection objectives," U.S. patent 20080037111A1 (February 14, 2008).
14. B. L. van der Waerden, *Group Theory and Quantum Mechanics* (Springer, 1974).